Angewandte Chemie
Eine Zeitschrift der Gesellschaft Deutscher Chemiker

Supporting Information

Room-Temperature Ferroelectricity in an Organic Cocrystal

Ren A. Wiscons[+], *N. Rajesh Goud*[+], *Joshua T. Damron, and Adam J. Matzger**

anie_201805071_sm_miscellaneous_information.pdf

Table of Contents

SI 1 | Experimental

Calculations. AN and F_4TCNQ were selected as cocrystallization partners based on gas phase calculations of the HOMO and LUMO energy levels, respectively (B3LYP/6-31G**). Using this method the HOMO-LUMO energy gap was calculated to be 0.23 eV (the HOMO-LUMO energy gap for TTF-CA is calculated at 0.24 eV, using the same method).

Sample preparation. Acenaphthene (Acros Organics) and d_{10}-acenaphthene (Sigma-Aldrich) were used as received, whereas F_4TCNQ (Ossila) was purified by zone sublimation to remove colored impurities before use. Single-crystals of AN-F_4TCNQ and d_{10}AN-F_4TCNQ were produced by slow evaporation from a 7.2 mM 1:1 stoichiometric ratio in acetonitrile (dried over molecular sieves) on polypropylene substrates. Single crystals were harvested and dried under vacuum before further characterization.

Single-Crystal Structure Determination. Single-crystal X-ray diffraction data for AN-F_4TCNQ was collected using a Rigaku AFC10K Saturn 944+ CCD-based X-ray diffractometer equipped with a low temperature device and Micromax-007HF Cu-target microfocus rotating anode (λ = 1.54187 Å) operated at 1.2 kW power (40 kV, 30 mA). X-ray intensities were measured at 85(1), 293(1), and 348(1) K with the detector placed 42.00 mm from the crystal. The data were processed with CrystalClear 2.0 (Rigaku)[1] and corrected for absorption. The structures were solved and refined with the Bruker SHELXTL (version 2008/4)[2] software package using direct methods. All non-hydrogen atoms were refined anisotropically with hydrogen atoms placed in a combination of refined and idealized positions. SCXRD data for d_{10}AN-F_4TCNQ was collected using a Rigaku XtaLAB Synergy-S X-ray diffractometer equipped with a low temperature device and a PhotonJet-S microfocus Cu source (λ = 1.54187 Å) operated at 50 kV and 1 mA. X-ray intensities were measured at 295(1) with the HyPix-6000HE detector placed 34.00 mm from the sample. The data were processed with CrysAlisPro v38.46 (Rigaku Oxford Diffraction) and corrected for absorption. The structures were solved in OLEX2[3] using SHELXTL[4] and refined using SHELXL.[5] All non-hydrogen atoms were refined anisotropically with hydrogen atoms placed in a combination of refined and idealized positions.

Powder X-ray diffraction. Variable-temperature powder XRD patterns were measured on a Rigaku R-Axis Spider diffractometer using Cu-Kα radiation (λ = 1.54187 Å) and operating at 40 kV and 44 mA. Samples were mounted on a CryoLoop™ and images were collected for 3 minutes with rotation of the sample about the ϕ-axis at 10°/sec, oscillating ω between 80° and 140° at 1°/sec with χ fixed at 45°. The sample collection temperature was set to temperatures between 295(1) and 348(1) K in 5 K increments via an Oxford Cryostream Plus Controller. The images were integrated from 2 to 50° with a 0.02° step size using AreaMax 2.0 software (Rigaku). The data were processed using Jade 8 XRD Pattern Processing, Identification & Quantification analysis software (Materials Data, Inc.).[6]

VT-Raman microscopy. Variable-temperature Raman spectra were collected using a Renishaw inVia Raman Microscope equipped with a Leica microscope, 785 nm laser, 1200 lines/mm grating, 65 μm slit, and a RenCam CCD detector. Calibration was performed using a silicon standard in static mode. Spectra were collected in static mode with the spectral window centered about 2200 cm^{-1} and analyzed using the WiRE 3.4 software package (Renishaw). The sample collection temperature was controlled by a Linkam Scientific TMS 94 hot stage attachment through the WiRE 3.4 collection software.

Electrical measurements. Electrical measurements were taken on single crystals contacted with silver paint. BFDH morphology prediction was produced by Mercury 3.7 offered by the CCDC and used to guide the placement of the electrode contacts on the (100) and (-100) faces. The *P-E* hysteresis loops were collected at room temperature on a ferroelectric testing probe station (Radiant Technologies Inc. Ferroelectric Test System) operated using Vision Data Acquisition Software (Radiant Technologies Inc.) using an alternating triangular double-wave field (preset-delay-measurement). PUND tests were also performed on single crystals using the Radiant Technologies Inc. Ferroelectric Testing System. The data provided in this manuscript were collected from two representative single crystals. Despite guidance from morphology predictions, contact placement was imperfect for several samples due to the blocky morphology of the crystal, and these samples showed unreliable and unsymmetrical polarization loops with no remanent behavior. It was concluded that, although sample measurements were reliable for well-placed electrodes, the *P-E* measurements are very specific to sample orientation.

Solid-state MAS-NMR. All ^{1}H NMR data was collected on a Bruker Avance III spectrometer at 400 MHz ^{1}H Larmor frequency using a Bruker 2.5mm probe under 20 kHz Magic Angle Spinning frequency. The probe temperature was calibrated using KBr[7] and the CS referenced to adamantane. The ^{1}H T_1 relaxation times were measured by saturation recovery with a 'Magic Sandwich Echo' before detection for background suppression and refocusing of some portion of the homonuclear dipolar coupling. The experiments were collected with 8 scans and a recycle delay of 5 s. The 1D spectra in the text and SI were taken from the final time point in the T_1 sequence at any given temperature. The saturation recovery experiments were assessed with a bicomponent fit, which modeled the data more appropriately than using a single component. The bimodal behavior of the curves are more pronounced at higher temperatures which can be seen in SI 20.

Material	AN-F_4TCNQ			d_{10}AN-F_4TCNQ
CCDC Number	1840749	1840751	1840750	1840748
Space Group	*Pc*	*Pc*	$P2_1/c$	*Pc*
a Å	9.37046(14)	9.4631(2)	9.4902(4)	9.46967(14)
b Å	7.91811(10)	7.98590(10)	8.0084(3)	7.98629(10)
c Å	13.2241(2)	13.3629(2)	13.5369(5)	13.37130(19)
α (°)	90	90	90	90
β (°)	110.4689(18)	109.407(2)	108.602(4)	109.3772(17)
γ (°)	90	90	90	90
Volume ($Å^3$)	919.23	952.475	975.074	953.957
Temperature	85(1)	293(1)	348(1)	293(2)
ρ_{calc} (g cm^{-3})	1.555	1.501	1.473	1.533
R_1/wR_2	4.00/10.92	3.18/9.19	7.35/23.81	3.13/10.49
GOF	1.039	1.053	1.086	1.136

SI 2 | Crystallographic parameters for AN-F_4TCNQ and d_{10}AN-F_4TCNQ. Crystal structures of AN-F4TCNQ were collected at 85, 293, and 348 K and the associated unit cell parameters and relevant statistics are shown in the table above. The unit cell parameters for d_{10}AN-F_4TCNQ are also given at room temperature.

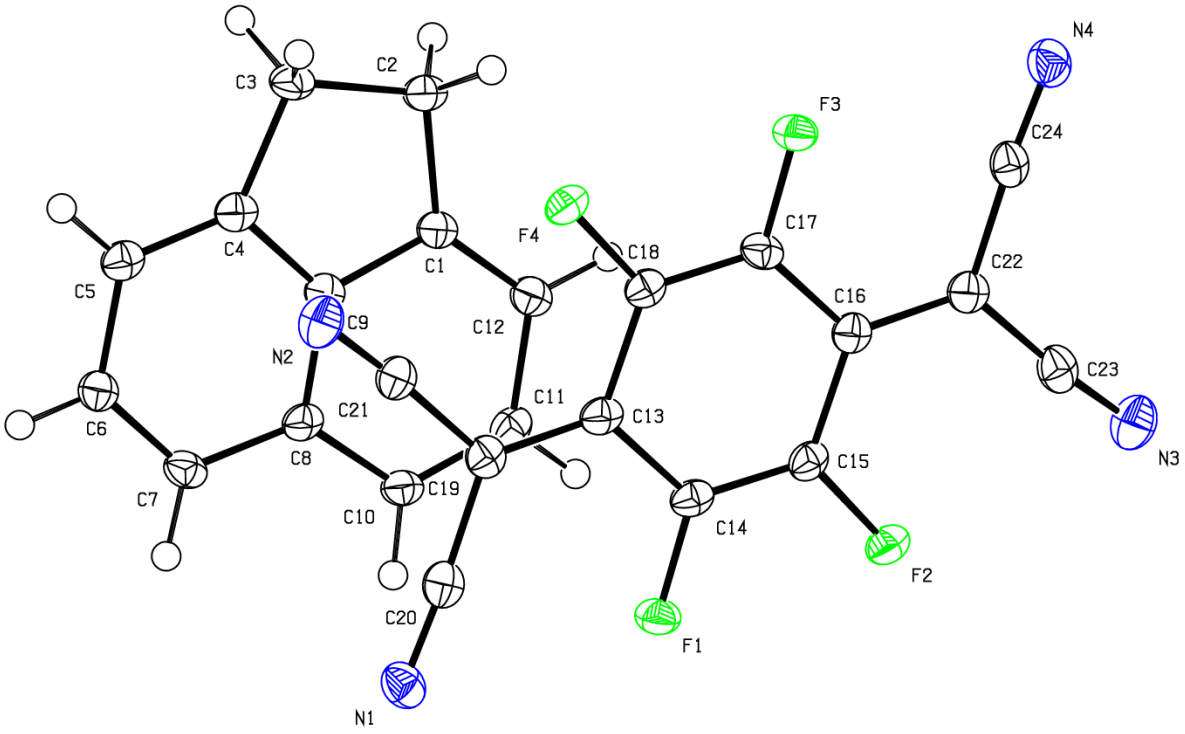

SI 3 | ORTEP diagram for AN-F4TCNQ at 85 K with thermal ellipsoids representing 50% probability.

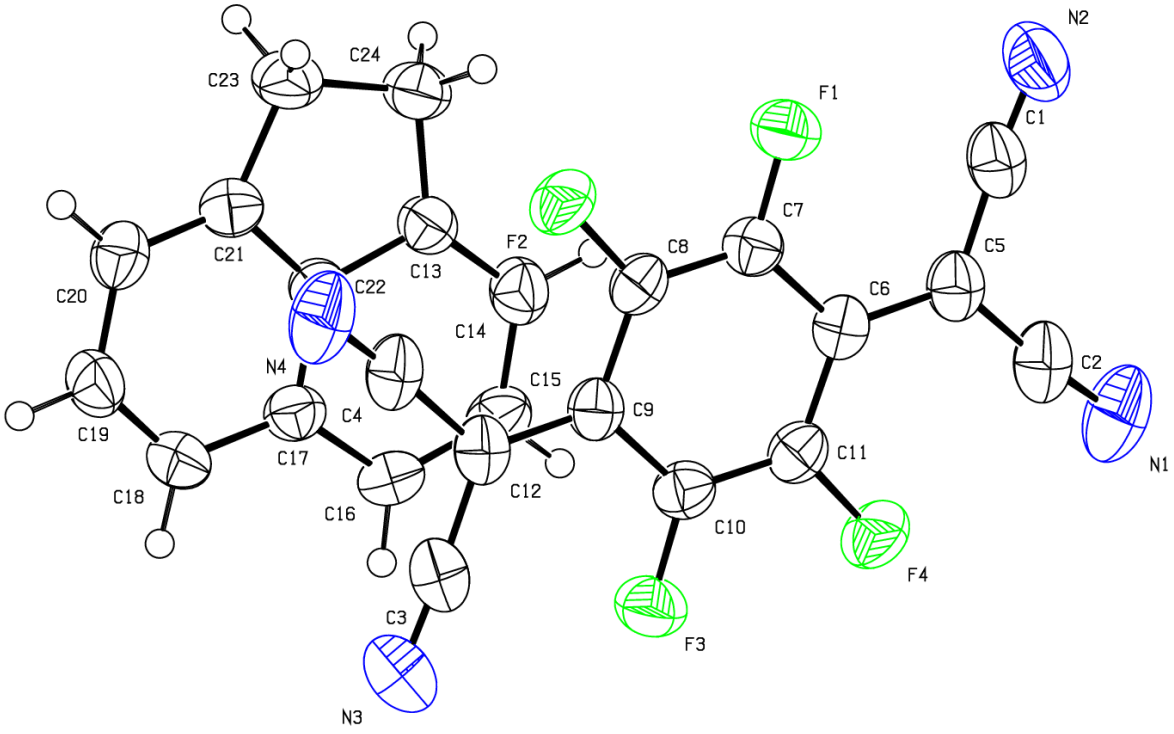

SI 3 | ORTEP diagram for AN-F4TCNQ at 293 K with thermal ellipsoids representing 50% probability.

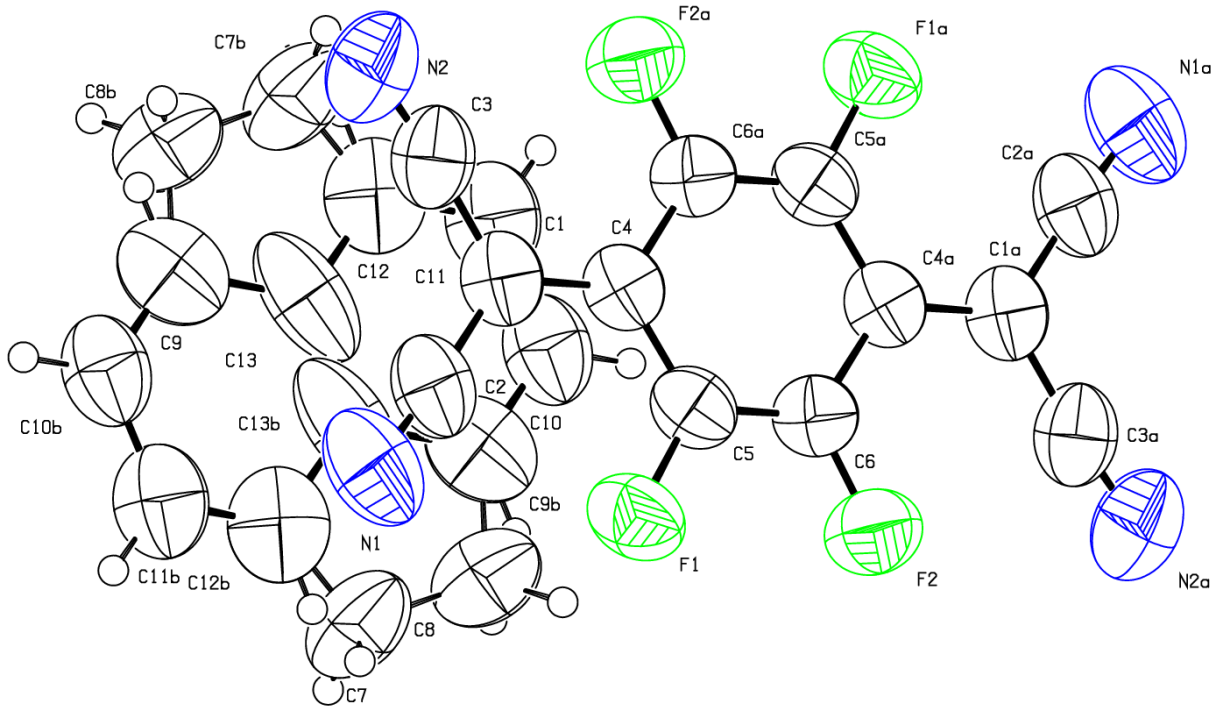

SI 3 | ORTEP diagram for AN-F4TCNQ at 348 K with thermal ellipsoids representing 50% probability.

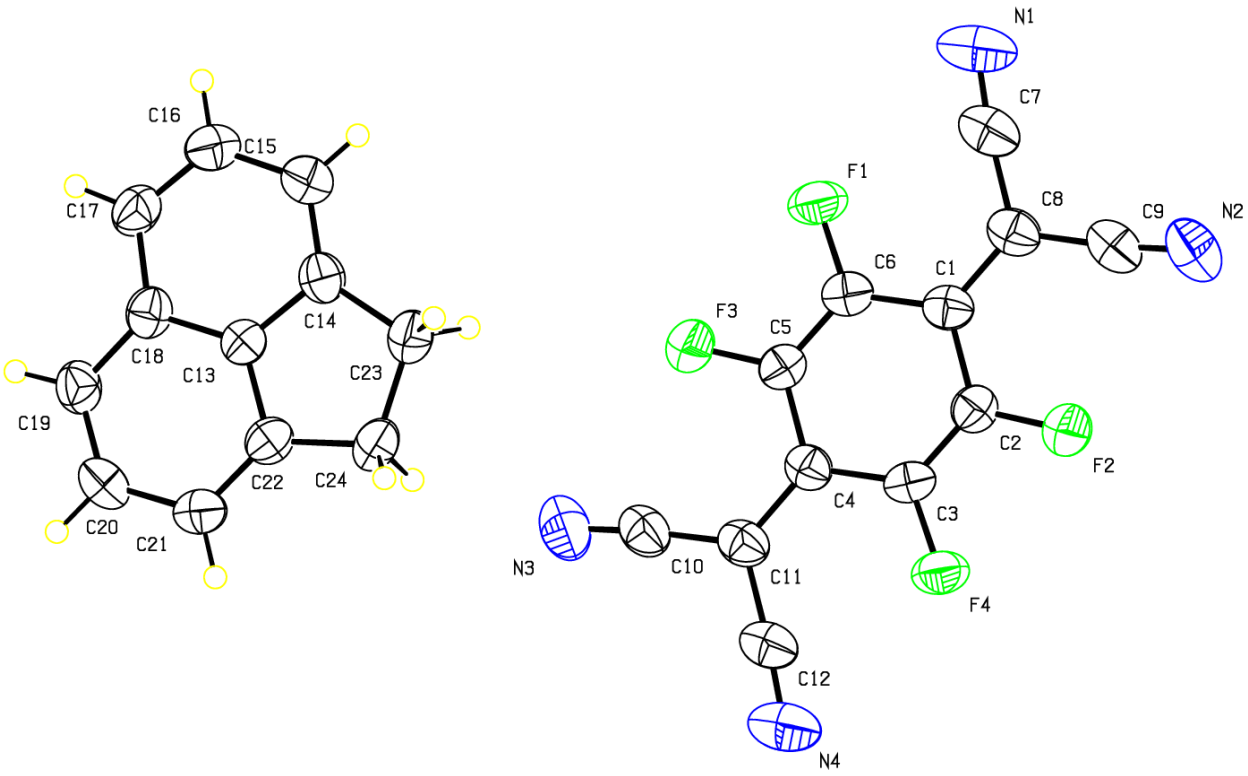

SI 4 | ORTEP diagram for d_{10}-AN-F4TCNQ at 293(2) K with thermal ellipsoids representing 50% probability.

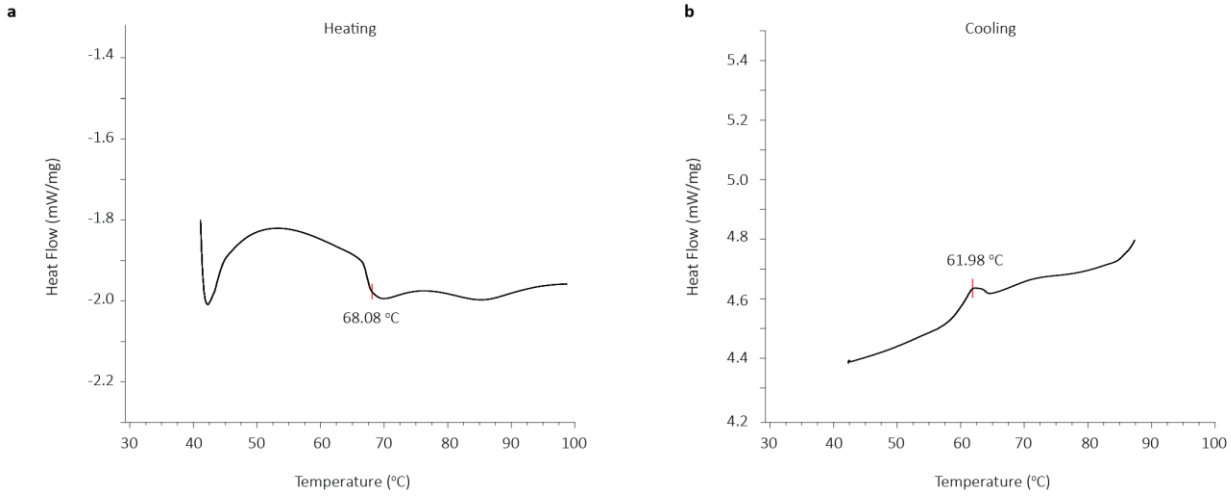

SI 5 | Differential scanning calorimetry trace for AN-F_4TCNQ. Typical cyclic DSC traces for AN-F_4TCNQ with **(a)** heating and **(b)** cooling events shown separately to magnify the endothermic and exothermic events. The endo- and exothermic peak maxima are labeled on the traces. Exothermic heat flow shown as upward peaks.

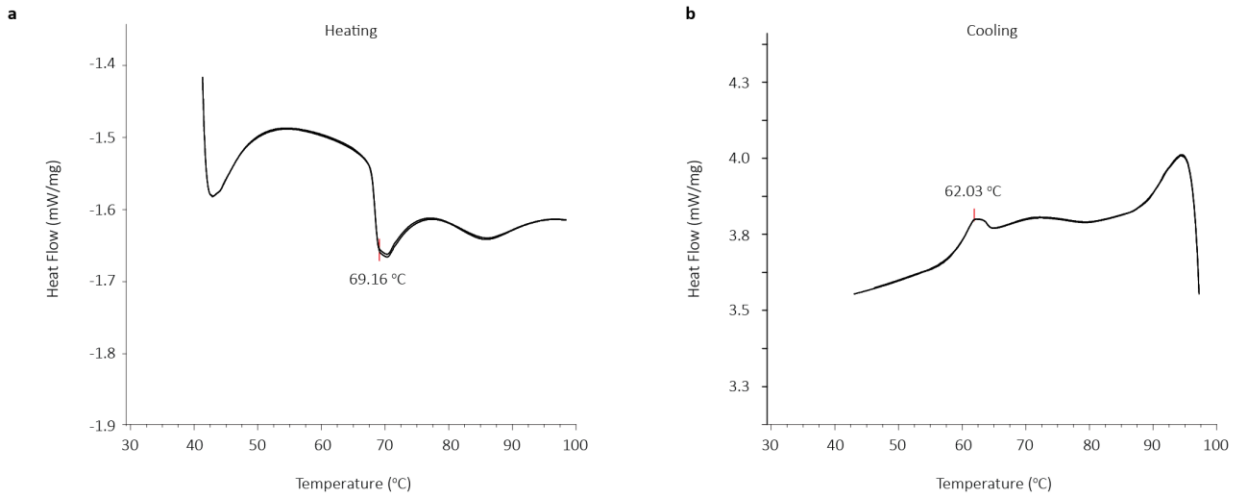

SI 6 | Differential scanning calorimetry trace for d_{10}AN-F_4TCNQ. Typical cyclic DSC traces for d_{10}AN-F_4TCNQ with **(a)** heating and **(b)** cooling events shown separately to magnify the endothermic and exothermic events. The endo- and exothermic peak maxima are labeled on the traces. Exothermic heat flow shown as upward peaks.

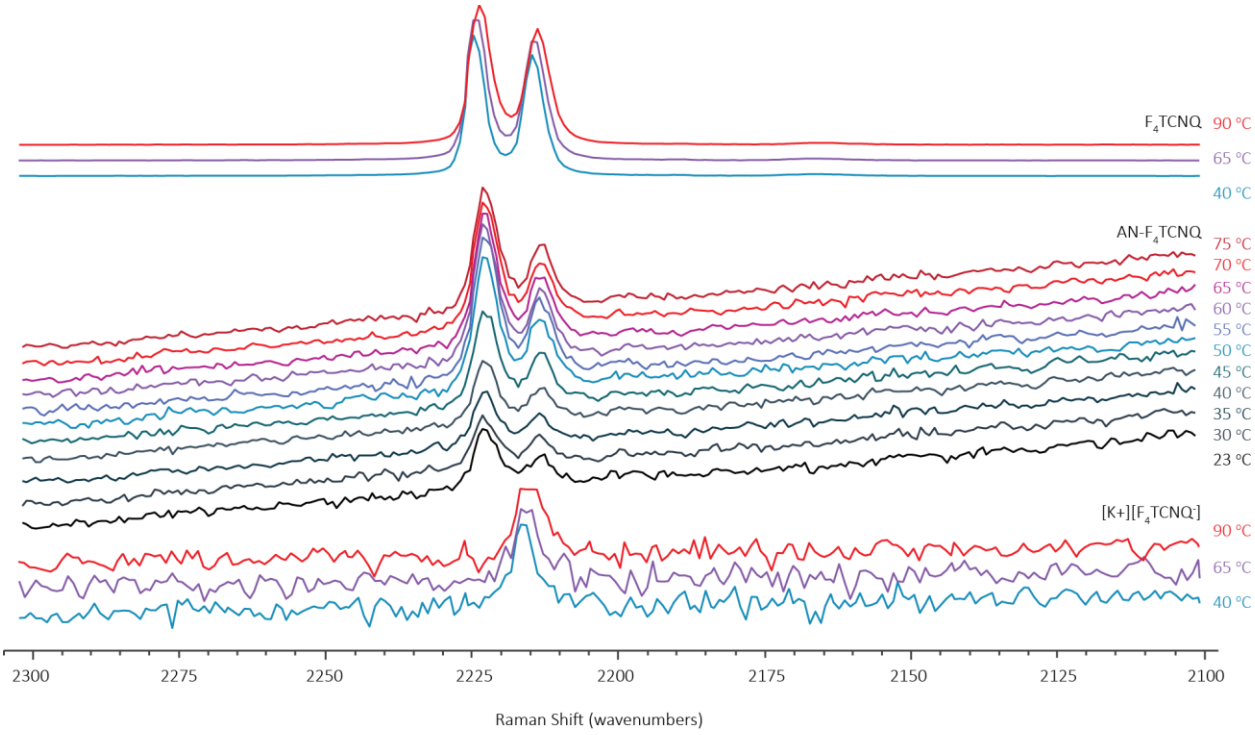

SI 7 | Static Raman spectra for AN-F_4TCNQ. Variable temperature Raman spectra for AN-F_4TCNQ between 23 and 75 °C as well as the neutral F_4TCNQ and radical anion [K^+][F_4TCNQ^-] standards at various temperatures for calculating ionicities/degree of charge transferred.

Temperature (°C)	*AN-F_4TCNQ (cm^{-1})*	*F_4TCNQ (cm^{-1})*	*[NEt_4][F_4TCNQ] (cm^{-1})*	*Ionicity (e)*
23	2223.23	2225.65	2217.66	0.30
30	2223.23	2225.65	2217.66	0.30
35	2222.82	2225.65	2217.66	0.35
40	2222.82	2225.65	2217.66	0.35
45	2223.03	2225.65	2217.66	0.33
50	2222.82	2225.65	2217.66	0.35
55	2223.03	2225.65	2217.66	0.33
60	2222.82	2225.65	2217.66	0.35
65	2222.82	2224.96	2217.66	0.30
70	2223.40	2224.96	2217.66	0.21
75	2223.40	2224.96	2217.66	0.21

SI 8 | Table of Raman peak values and calculated ionicities. The ionicities were calculated using $\rho = 2(\nu_0 - \nu_{CT}) / \nu_0(1 - \nu_1^2/ \nu_0^2)^{-1}$ where ν_0, ν_{CT}, and ν_1 are the–CN stretching frequencies in the neutral standard, CT sample, and radical anion standard, respectively.

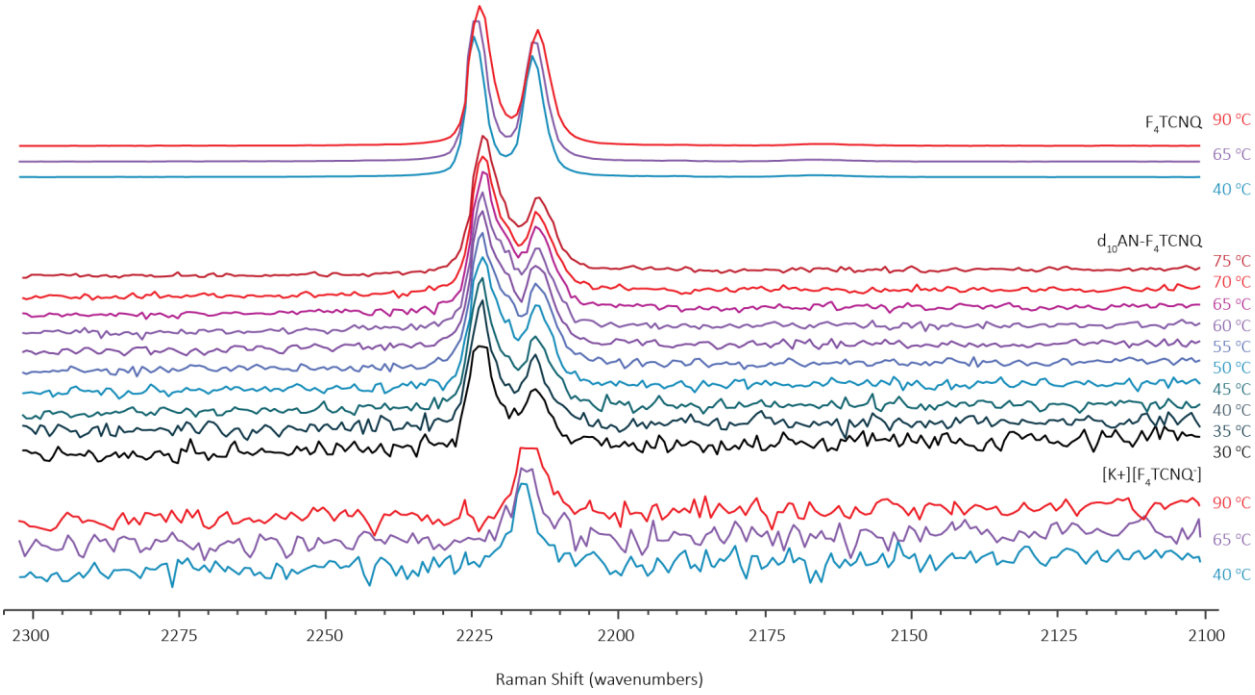

SI 9 | Static Raman spectra for d_{10}AN-F_4TCNQ. Variable temperature Raman spectra for d_{10}AN-F_4TCNQ between 23 and 75 °C as well as the neutral F_4TCNQ and radical anion [K^+][F_4TCNQ^-] standards at various temperatures for calculating ionicities/degree of charge transferred.

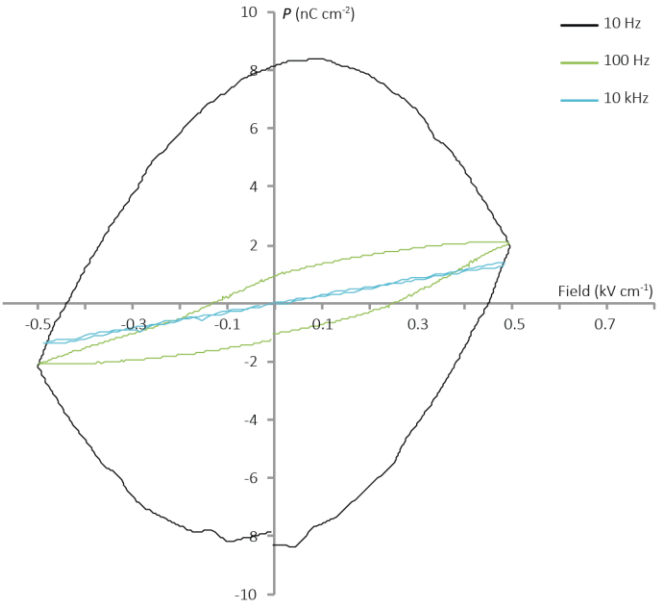

SI 10 | Typical standard bipolar hysteresis plot for AN-F_4TCNQ at room temperature. Typical polarization measured directly (non-PUND) from AN-F_4TCNQ using a standard bipolar sequence (drive voltage of 15 V) showing strong frequency dependence.

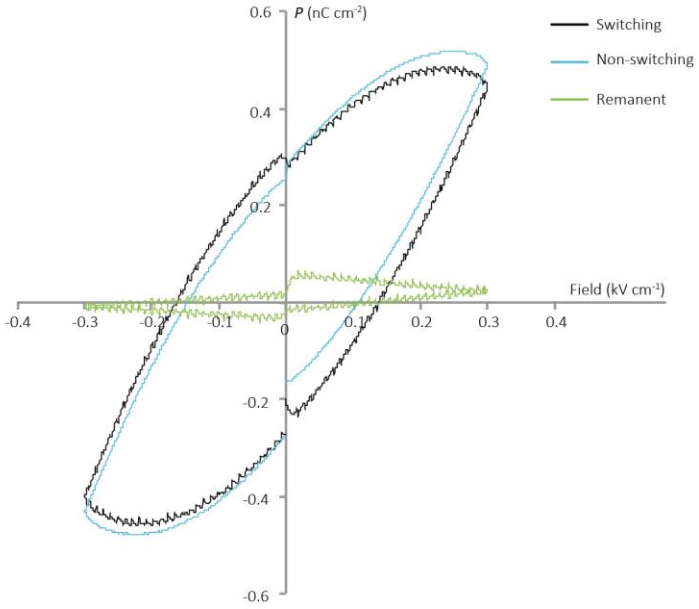

SI 11 | Remanent polarization hysteresis plot for AN-F_4TCNQ. Sample remanent hysteresis plot for AN-F_4TCNQ constructed from two (positive and negative) remanent hysteresis half loops. The switching (black) loop includes dielectric and hysteresis contributions, the non-switching (blue) loop includes only dielectric contributions, and the remanent loop is the calculated hysteresis.

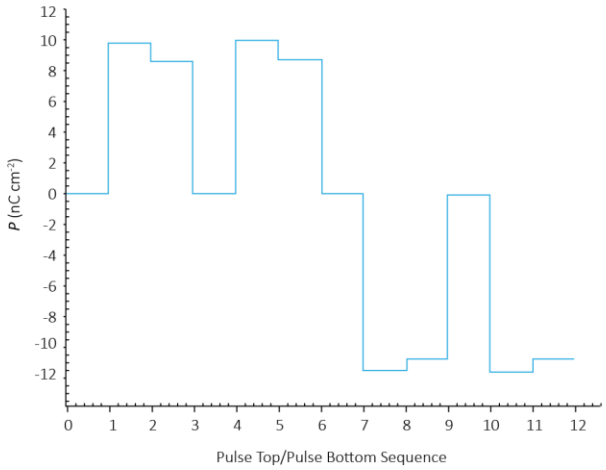

SI 12 | Sample PUND pulse profile for AN-F$_4$TCNQ at room temperature. Example of AN-F$_4$TCNQ polarization measured against the PUND pulse sequence.

Area (cm^2)	Separation (μm)	E Field (kV/cm)	Delay (ms)	Pulse Width (ms)	d*P*r ($nC\ cm^{-2}$)
0.048	500	0.35	1000	0.01	0.02
0.048	500	0.35	1000	0.50	0.06
0.048	500	0.35	1000	1.00	0.08
0.048	500	0.35	1000	2.50	0.03
0.048	500	0.35	1000	5.00	-0.03

SI 13 | Sample PUND data for AN-F_4TCNQ at room temperature. Pulse width-dependent remnant polarization values (d*P*r) for AN-F_4TCNQ measured by PUND.

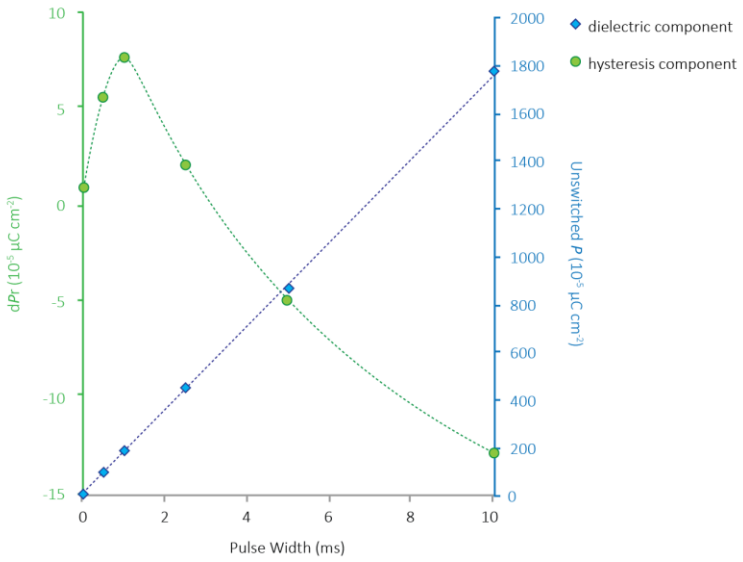

SI 14 | Pulse width-dependent dielectric and ferroelectric contributions to polarization for AN-F_4TCNQ. Dielectric and hysteresis (ferroelectric) component polarization intensities as a function of pulse width.

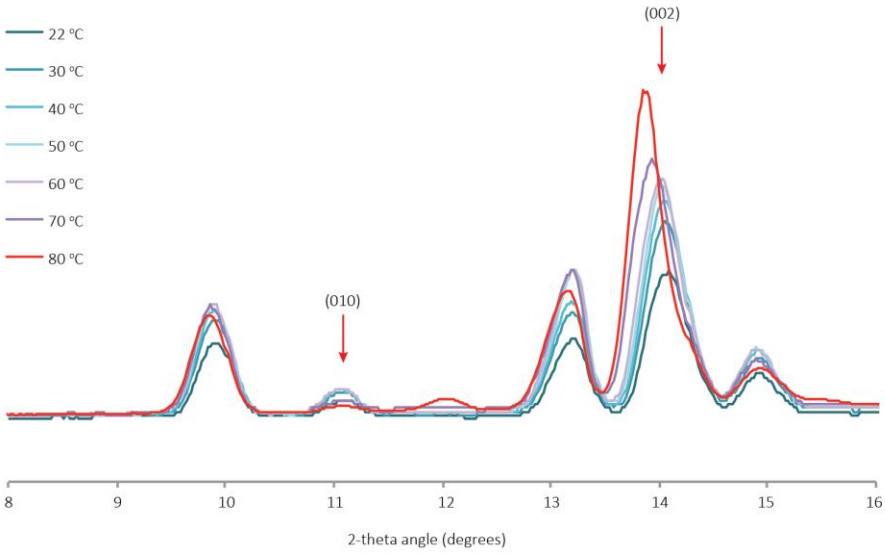

SI 15 | VT-PXRD patterns for AN-F_4TCNQ. PXRD patterns of AN-F_4TCNQ taken between 22 and 80 °C highlighting the two reflections, the (010) and (002), monitored for the ferroelectric mechanistic studies.

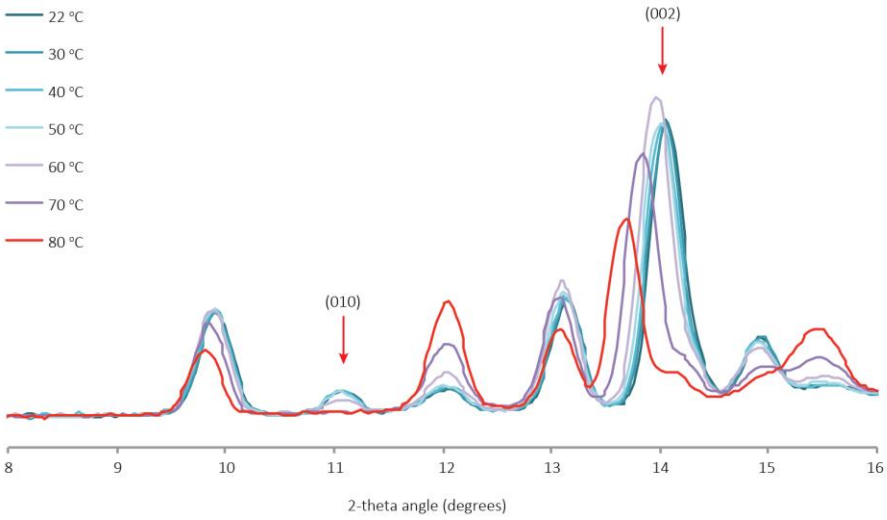

SI 16 | VT-PXRD patterns for d_{10}AN-F_4TCNQ. PXRD patterns of d_{10}AN-F_4TCNQ taken between 22 and 80 °C highlighting the two reflections, the (010) and (002), monitored for the ferroelectric mechanistic studies.

Temp (°C)	(002) H_{10}-2θ (°)	(002) d_{10}-2θ (°)	(002) H_{10}-d (Å)	(002) d_{10}-d (Å)	(010) H_{10}-2θ (°)	(010) d_{10}-2θ (°)	(010) H_{10}-d (Å)	(010) d_{10}-d (Å)
22	14.070	14.066	6.289	6.291	11.077	11.078	7.981	7.980
30	14.044	14.047	6.301	6.300	11.063	11.069	7.991	7.987
40	14.038	14.026	6.303	6.309	11.058	11.061	7.995	7.993
50	14.021	14.009	6.311	6.317	11.055	11.047	7.997	8.003
60	14.010	13.968	6.316	6.335	11.045	11.073	8.005	7.984
70	13.925	13.840	6.355	6.393	11.040		8.008	
80	13.862	13.679	6.383	6.468	11.073		7.984	

SI 17 | Peak positions and d-spacings for AN-F_4TCNQ and d_{10}AN-F_4TCNQ VT-PXRD. VT-PXRD 2θ and d-spacings for AN-F_4TCNQ and d_{10}AN-F_4TCNQ.

Temp (°C)	*a* (Å)	*b* (Å)	*c* (Å)	(002) (Å)	β (°)	V (Å^3)
22(1)	9.462(4)	7.987(4)	13.368(6)	6.684(6)	109.46(4)	952.5(7)
30(1)	9.470(5)	7.986(5)	13.374(7)	6.687(7)	109.40(4)	954.3(7)
40(1)	9.476(4)	8.001(4)	13.381(4)	6.691(4)	109.31(4)	957.5(7)
50(1)	9.479(4)	8.001(6)	13.404(5)	6.702(5)	109.21(4)	960.0(9)
60(1)	9.482(5)	8.011(3)	13.451(5)	6.708(5)	109.13(4)	962.8(7)
70(1)	9.482(5)	8.013(5)	13.486(7)	6.743(7)	108.86(5)	969.6(9)
80(1)	9.494(5)	7.999(4)	13.550(7)	6.775(7)	108.55(4)	976.4(8)

SI 18 | Unit cell parameters for AN-F_4TCNQ collected by VT-SCXRD.

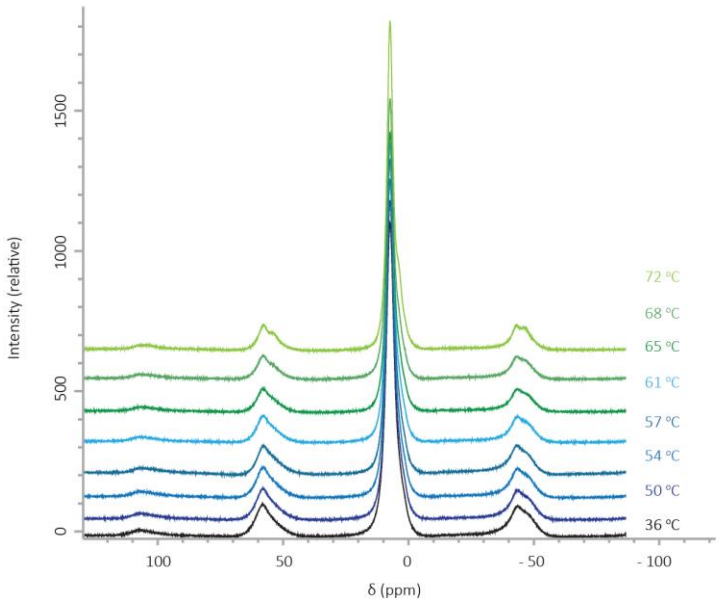

SI 19 | ^{1}H SS MAS-NMR spectra for AN-F_4TCNQ. 1D ^{1}H SS MAS-NMR spectra for AN-F_4TCNQ taken between 36 and 72 °C.

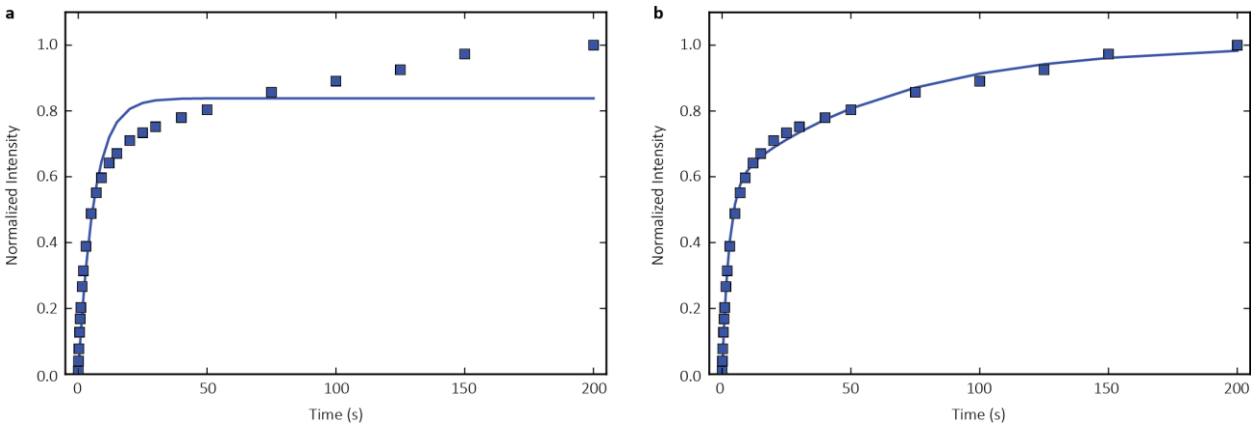

SI 20 | (a) Single and (b) bicomponent fits for MAS NMR saturation recovery data at 72 °C.

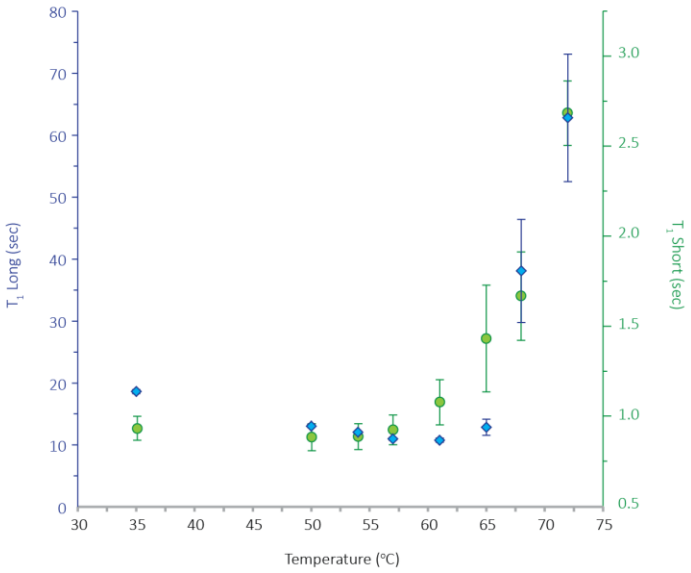

SI 21 | VT-T_1 relaxation times for AN-F_4TCNQ. Bulk T_1 relaxation times as a function of temperature fit with a bicomponent analysis with the long component displayed in blue and the short component displayed in green.

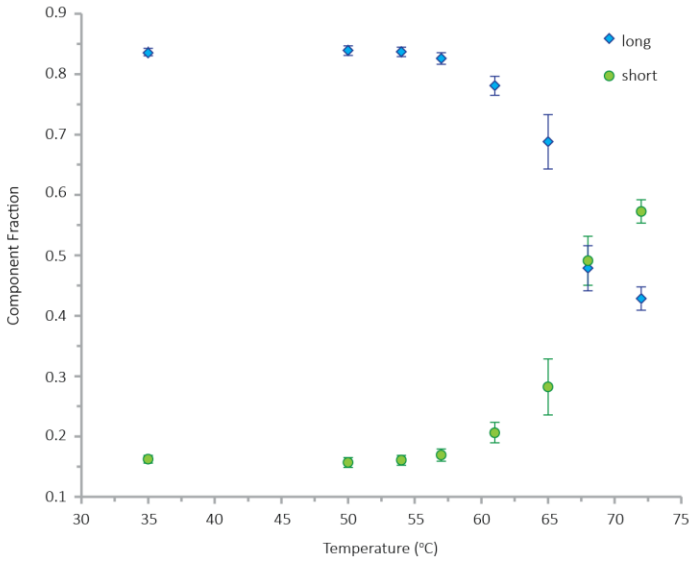

SI 22 | Long and short T_1 component fractions as a function of temperature. The long, blue, and short, green, component fractions as a function of temperature for the bicomponent fit of the T_1 relaxation data.

SI 23 | References

[1] CrystalClear Expert 2.0 r12, Rigaku Americas and Rigaku Corporation (2011), Rigaku Americas, 9009, TX, USA 77381-5209, Rigaku Tokyo, 196-8666, Japan.

[2] G. M. Sheldrick, SHELXTL, v. 2008/4; Bruker Analytical X-ray, Madison, WI, 2008.

[3] O. V. Dolomanov, L. J. Bourhis, R. J. Gildea, J. A. K. Howard, H. Puschmann, *J. Appl. Cryst.* **2009**, *42*, 339-341.

[4] G. M. Sheldrick, *Acta Cryst. A* **2015**, *71*, 3-8.

[5] G. M. Sheldrick, *Acta Cryst. C* **2015**, *71*, 3-8.

[6] Jade Plus 8.2 ed.; Materials Data, Inc. 1995-2007.

[7] K. R. Thurber, R. Tycko, *J. Magn. Reson.* **2009**, *196*, 84–87.